VOL. 18, NO. 6, MARCH 2023 ISSN 1819-6608
ARPN Journal of Engineering and Applied Sciences

www.arpnjournals.com

NUMERICAL ANALYSIS ON THE EFFECT OF DILUTED HYDROGEN FUEL BY A FIXED AMOUNT OF SUPPLIED HYDROGEN USING A QUASI-THREE-DIMENSIONAL SOLID OXIDE FUEL CELL MODEL

W. C. Tan[1,2], E. A. Lim[3], E. M. Cheng[4], W. H. Tan[1] and H. A. Rahman[5]
[1]Faculty of Mechanical Engineering and Technology, Universiti Malaysia Perlis, Pauh Putra Campus, Arau, Perlis, Malaysia
[2]Thermofluids and Energy Research Group, Universiti Malaysia Perlis, Pauh Putra Campus, Arau, Perlis, Malaysia
[3]Institute of Engineering Mathematics, Universiti Malaysia Perlis, Arau, Perlis, Malaysia
[4]Faculty of Electronic Engineering and Technology, Universiti Malaysia Perlis, Pauh Putra Campus, Arau, Perlis, Malaysia
[5]Faculty of Mechanical and Manufacturing Engineering, Universiti Tun Hussein Onn Malaysia, Parit Raja, Johor, Malaysia
E-Mail: tweechoon@unimap.edu.my

ABSTRACT

Solid oxide fuel cell (SOFC) has excellent fuel flexibility for various fuels. Despite some drawbacks like storage and transportation, hydrogen stands up as the best fuel for SOFC. Hydrogen fuel is diluted non-reactive gas species before it is supplied to the SOFC. In this study, a quasi-three-dimensional SOFC model with real microstructure is used to analyse the effect of the diluted fuel mixture. The hydrogen fuel is diluted with nitrogen and a small amount of steam. The mole amount of hydrogen within fuel mixtures is kept constant. On the other hand, the air that is supplied to the air channel of the SOFC remains unchanged. It is found that the cell that is supplied with the highest concentration of hydrogen has the highest performance due to its high partial pressure of hydrogen within the fuel mixture. Such a high partial pressure promotes a low anode concentration loss. Also, the cell that is supplied with a low hydrogen concentration is unable to benefit from its high average cell temperature as its performance is drained by the low partial pressure of hydrogen within the fuel mixture.

Keywords: dusty gas model, performance analysis, area-specific resistance, heat generation.

1. INTRODUCTION

Hydrogen and oxygen are supplied to a solid oxide fuel cell (SOFC) to convert chemical energy to electrical energy through electrochemical processes. The oxidation reaction of hydrogen and the reduction reaction of oxygen which are half-reactions of the electrochemical reaction need to be separated to allow the transportation of electrons through an external circuit as electrical work. Therefore, hydrogen is supplied through the fuel channel, whereas oxygen is supplied in the air channel. Instead of pure oxygen, the air channel mostly is supplied with ambient air. The additional component of nitrogen within the ambient air helps to reduce the heat within SOFC. On the other hand, the hydrogen is humidified at a minimum level for safety reasons. The humidified hydrogen fuel can be further diluted by adding non-reactive gas species such as nitrogen.

Yahya *et al.* [1] conducted an electrochemical analysis of the performance of an SOFC. In their analysis, the effects of hydrogen molar fraction and the volume flow rate of the supplied fuel of hydrogen-steam, hydrogen-nitrogen and hydrogen-nitrogen-steam mixtures towards the performance of the SOFC were investigated. Both steam and nitrogen are acted as an agent to dilute the supplied hydrogen fuel. Wu *et al.* [2] experimentally spatially resolved the electrochemical performance and temperature distribution within an SOFC under the influence of hydrogen dilution ratios and electrical loadings. The hydrogen fuel was also diluted with the concentration of 97%, 48.5% and 19.4% with nitrogen and steam. Komatsu *et al.* [3]experimental investigated fuel provision control and the transient capability of cell performance on the 300W stack with 50% - 70% diluted hydrogen fuel under a fixed volume flow rate. Brus *et al.* [4] numerically investigate the effect of tortuosity of an anode in comparison between the value obtained from saturation currents as well as the mass transport model and real microstructure. The current-voltage characteristics of an SOFC are analysed with the supplied hydrogen-nitrogen-steam ternary system with 2.5% - 90% hydrogen at the operating temperature of 923 K and 1023 K. All the above studies show that the performance of the cell is degraded when the supplied hydrogen is diluted. Also, the supplied mole amount of hydrogen within various supplied fuel mixtures is found to vary with each other under the constant volume flow rate. It is expected that a cell with a low molar fraction of hydrogen has a low amount of hydrogen. In this case, the heat generated is limited by the electrochemical reaction and results in a low cell temperature which degrades the performance of the cell.

The numerical analysis allows researchers to understand the complex phenomena of heat, mass and charge transport in SOFCs. A quasi-3D SOFC model was previously developed and used for the analysis of intermediate-temperature direct-internal-reforming SOFC [5]. This quasi-3D SOFC model with real microstructure information was developed in the authors' group to study the effect of cell aspect ratio on cell performance [6] and the effects of the air-flow configuration in a short stack [7]. In this work, the ternary fuel mixture of hydrogen, nitrogen and steam with various molar fractions is supplied to a SOFC to study the influence of the fuel

mixture under a constant mole amount of hydrogen within the supplied fuel.

2. NUMERICAL MODELLING

A cell unit as shown in Figure-1(a) consists of top and bottom separators, fuel and air channels, and a positive-electrolyte-negative assembly (PEN) is considered in this study. Each component has only one mesh on the *y*-axis. Note that both fuel and air channels consist of solid- and fluid-phase meshes as shown in Figure-1(b). The cell has an effective area of 80.0×60.0 mm^2. Details of the quasi-3D SOFC model have already been described in our previous reports [6][7][8], therefore only essential equations are summarized below.

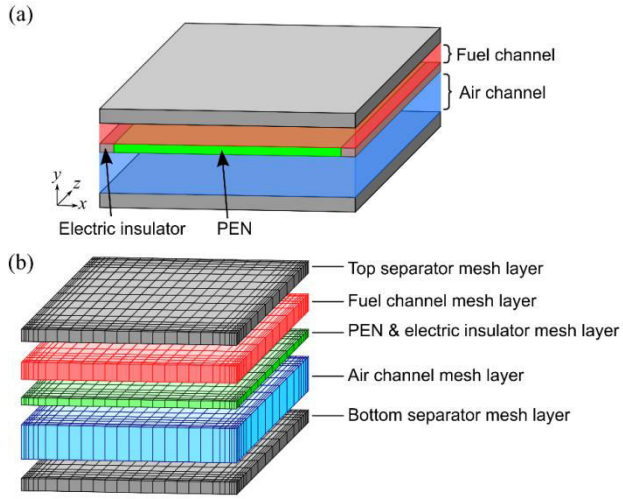

Figure-1. Schematic view of (a) cell unit and (b) mesh layers for quasi-3D SOFC model. Governing equations.

The numerical analysis was based on conservation equations of mass, momentum, species, and energy.

Mass conservation:

$$\frac{\partial(\rho u)}{\partial x}+\frac{\partial(\rho w)}{\partial z}=\sum S_{Y_i} \quad (1)$$

Momentum conservation:

$$\left[\frac{\partial}{\partial x}\left(\frac{\rho uu}{\varepsilon}\right)+\frac{\partial}{\partial z}\left(\frac{\rho wu}{\varepsilon}\right)\right]=-\varepsilon\frac{\partial P}{\partial x}+\frac{\partial}{\partial x}\left(\mu\frac{\partial u}{\partial x}\right)+\frac{\partial}{\partial z}\left(\mu\frac{\partial u}{\partial z}\right)+\frac{1}{3}\frac{\partial}{\partial x}\left(\mu\frac{\partial u}{\partial x}\right)-\frac{2}{3}\frac{\partial}{\partial x}\left(\mu\frac{\partial w}{\partial z}\right)+\frac{\partial}{\partial z}\left(\mu\frac{\partial w}{\partial x}\right)-\varepsilon\frac{\mu}{K}u-\varepsilon\frac{\rho f}{\sqrt{K}}|U|u \quad (2)$$

$$\left[\frac{\partial}{\partial x}\left(\frac{\rho uw}{\varepsilon}\right)+\frac{\partial}{\partial z}\left(\frac{\rho ww}{\varepsilon}\right)\right]=-\varepsilon\frac{\partial P}{\partial z}+\frac{\partial}{\partial x}\left(\mu\frac{\partial w}{\partial x}\right)+\frac{\partial}{\partial z}\left(\mu\frac{\partial w}{\partial z}\right)+\frac{1}{3}\frac{\partial}{\partial z}\left(\mu\frac{\partial w}{\partial z}\right)-\frac{2}{3}\frac{\partial}{\partial z}\left(\mu\frac{\partial u}{\partial x}\right)+\frac{\partial}{\partial x}\left(\mu\frac{\partial u}{\partial z}\right)-\varepsilon\frac{\mu}{K}w-\varepsilon\frac{\rho f}{\sqrt{K}}|U|w \quad (3)$$

Energy conservation:
(fluid phase in the channels filled with metal foam)

$$\frac{\partial(\rho C_p uT_\mathrm{f})}{\partial x}+\frac{\partial(\rho C_p wT_\mathrm{f})}{\partial z}=\frac{\partial}{\partial x}\left(\lambda_\mathrm{f}^{\mathrm{eff}}\frac{\partial T_\mathrm{f}}{\partial x}\right)+\frac{\partial}{\partial z}\left(\lambda_\mathrm{f}^{\mathrm{eff}}\frac{\partial T_\mathrm{f}}{\partial z}\right)+h_{\mathrm{sf}}a_{\mathrm{sf}}(T_\mathrm{s}-T_\mathrm{f}) \quad (4)$$

(solid phase in the channels filled with metal foam)

$$0=\frac{\partial}{\partial x}\left(\lambda_\mathrm{s}^{\mathrm{eff}}\frac{\partial T_\mathrm{s}}{\partial x}\right)+\frac{\partial}{\partial z}\left(\lambda_\mathrm{s}^{\mathrm{eff}}\frac{\partial T_\mathrm{s}}{\partial z}\right)+h_{\mathrm{sf}}a_{\mathrm{sf}}(T_\mathrm{f}-T_\mathrm{s}) \quad (5)$$

(solid phases in the separator and the cell)

$$0=\frac{\partial}{\partial x}\left(\lambda_\mathrm{s}\frac{\partial T_\mathrm{s}}{\partial x}\right)+\frac{\partial}{\partial z}\left(\lambda_\mathrm{s}\frac{\partial T_\mathrm{s}}{\partial z}\right)+Q \quad (6)$$

Species conservation:

$$\frac{\partial}{\partial x}(\rho uY_i)+\frac{\partial}{\partial z}(\rho wY_i)=\frac{\partial}{\partial x}\left(\rho D_{i,\mathrm{m}}^{\mathrm{eff}}\frac{\partial Y_i}{\partial x}\right)+\frac{\partial}{\partial z}\left(\rho D_{i,\mathrm{m}}^{\mathrm{eff}}\frac{\partial Y_i}{\partial z}\right)+S_{Y_i} \quad (7)$$

Charge conservation

$$\frac{\partial}{\partial x}\left(\sigma_\mathrm{s}^{\mathrm{eff}}\frac{\partial\phi}{\partial x}\right)+\frac{\partial}{\partial y}\left(\sigma_\mathrm{s}^{\mathrm{eff}}\frac{\partial\phi}{\partial y}\right)+\frac{\partial}{\partial z}\left(\sigma_\mathrm{s}^{\mathrm{eff}}\frac{\partial\phi}{\partial z}\right)=S_\phi \quad (8)$$

The validation of the developed quasi-3D SOFC model with the updated DGM within electrodes was conducted in our previous works [8]. An in-house Fortran code is developed and run with a laptop that is equipped with an Intel i5 processor 1.7 GHz and 12 GB RAM.

2.1 Dusty Gas Model

Dusty-gas model (DGM) is implemented for the transport of reactants and product in the porous anode. DGM can be expressed as follows [9]:

$$\frac{N_i}{D_{\mathrm{K},i}^{\mathrm{eff}}}+\sum_{i\neq j}\frac{x_jN_i-x_iN_j}{D_{ij}^{\mathrm{eff}}}=-\frac{P}{RT_\mathrm{s}}\nabla x_i-\frac{x_i}{RT_\mathrm{s}}\left(1+\frac{KP}{\mu D_{\mathrm{K},i}^{\mathrm{eff}}}\right)\nabla P \quad (9)$$

$$\nabla P=-\frac{\sum\frac{N_i}{D_{\mathrm{K},i}^{\mathrm{eff}}}}{\frac{1}{RT_\mathrm{s}}+\frac{K}{\mu}\sum x_iD_{\mathrm{K},i}^{\mathrm{eff}}} \quad (10)$$

$$D_{\mathrm{K},i}^{\mathrm{eff}}=\frac{2}{3}\left(\frac{8RT_\mathrm{s}}{\pi M_i}\right)^{1/2}\bar{r} \quad (11)$$

where, x_i, N_i and M_i are the molar fraction, the molar flux and the molecular mass of gas species, respectively. μ, R, T_s and P are the viscosity, gas constant, temperature and total pressure of the gas mixture. ∇P is the pressure gradient. $\bar{r}$ is the average radius of the pore in an electrode. The permeability constant in the porous medium K and the effective binary gas diffusion D_{ij}^{eff} are described in [10].

2.2 Microstructure Information

The validation of the developed numerical model is conducted with the real microstructure which is manufactured by SOLID power S.p.A. with nickel - yttria-stabilized zirconia (Ni-YSZ) anode, YSZ electrolyte, gadolinium-doped ceria (GDC) barrier layer, lanthanum strontium cobalt ferrite (LSCF) - GDC function layer of cathode and LSCF current collector layer of LSCF. The

cell has an effective area of 80 mm × 60 mm with a thickness of 240, 8, 4, and 50 μm for the anode, electrolyte, GDC barrier layer, and cathode layer, respectively. The details of the microstructure are given in [6].

2.3 Calculation Conditions

The fuel channel is supplied with a constant mass flow rate of fuel mixture with a molar fraction ratio as shown in Table-1. The supplied fuel mixture is ensured with the same amount of 0.2064 mol s^{-1} for the supplied hydrogen within the fuel mixture. On the other hand, the same constant mass flow rate of 6.09×10^{-5} kg $s^{-1}$and molar fraction ratios of 0.210:0.790 for oxygen (O_2): nitrogen (N_2) is supplied for all numerical analyses. The outlet pressure of both the fuel and air mixture is maintained at the atmospheric pressure.

Table-1. Fuel mixture.

Molar fraction of H_2: N_2: H_2O	Mass flow rate [kg s^{-1}]
0.10: 0.88: 0.02	5.20×10^{-5}
0.20: 0.78: 0.02	2.33×10^{-5}
0.30: 0.68: 0.02	1.38×10^{-5}
0.40: 0.58: 0.02	8.99×10^{-6}
0.50: 0.48: 0.02	6.12×10^{-6}
0.60: 0.38: 0.02	4.20×10^{-6}
0.70: 0.28: 0.02	2.83×10^{-6}
0.80: 0.18: 0.02	1.81×10^{-6}
0.90: 0.08: 0.02	1.01×10^{-6}

The boundary conditions for the validation with the experimental [6] are given in Table-2. Note that the electric potential difference between the top and bottom separators is the terminal voltage of the cell unit and is iteratively tuned to achieve a pre-determined average current density. The pressure fields in the fuel and air channels are solved by the semi-implicit method for the pressure-linked equations (SIMPLE) algorithm.

4. RESULTS AND DISCUSSIONS

The numerical results in this work are conducted at temperatures of 973 K. Figure-3 shows the performance of the cell under various supplied fuel mixtures as given in Table-2. The solid lines show the current-voltage characteristics of the cell under the effect of the fuel mixture. In contrast, the dash lines show the power-current density characteristics. Although all fuel mixtures are supplied with the same amount of hydrogen for the electrochemical reaction within SOFC, the fuel mixture with a rich H_2 ratio (0.90 H_2: 0.08 N_2: 0.02 H_2O) shows excellent performance among all fuel mixtures. Such observation in Figure-3 is found similar with the experimental study on the hydrogen concentration between 50% to 70% under constant volume flow rate with a 300W class planar type SOFC stack by Komatsu *et al.* [3], where a cell that is supplied with a high hydrogen concentration leads to a high cell performance.

Table-2. Boundary conditions.

	$\boldsymbol{u}$	$\boldsymbol{W}$	$\boldsymbol{T_f}$	$\boldsymbol{T_s}$	$\boldsymbol{Y_i}$	$\boldsymbol{\phi}$
Inlet	$u = u_{in}$	$w = 0$	$T_f = T_{in}$	$\frac{\partial T_s}{\partial x} = 0$	$Y_i = Y_{i,\,in}$	$\frac{\partial \phi}{\partial x} = 0$
Outlet	$\frac{\partial u}{\partial x} = 0$	$\frac{\partial w}{\partial x} = 0$	$\frac{\partial T_f}{\partial x} = 0$	$\frac{\partial T_s}{\partial x} = 0$	$\frac{\partial Y_i}{\partial x} = 0$	$\frac{\partial \phi}{\partial x} = 0$
Wall	$u = 0$	$w = 0$	$\frac{\partial T_f}{\partial z} = 0$	$\frac{\partial T_s}{\partial z} = 0$	$\frac{\partial Y_i}{\partial z} = 0$	$\frac{\partial \phi}{\partial z} = 0$

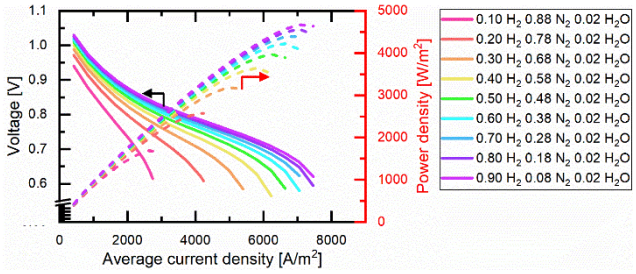

Figure-2. Comparison of current-voltage characteristics.

Area-specific resistance (ASR) analysis is conducted at the fuel utilization of 75% where the average current density is 6222.83 A/m^2. Note that a cell with a low hydrogen molar fraction (below 0.40) is unable to perform at this high average current density as shown in the current-voltage characteristics in Figure-2. The ASR analysis is shown in Figure-3. From the lowest of the stacked bar chart is the ASR value for anode activation, followed by anode ohmic loss, anode concentration, electrolyte ohmic loss, cathode activation, cathode ohmic loss and cathode concentration. It is found that the cell with the highest hydrogen molar fraction has the lowest total ASR value. When the hydrogen molar fraction is decreased in the fuel mixture, it leads to a decrease in the partial pressure of the hydrogen. This leads to an increment of the concentration loss in the anode. Although a cell with a low hydrogen molar fraction has a high ASR value for the anode concentration, this voltage loss is not converted to heat as waste. This is due to this voltage loss being related to the energy loss that is converted to additional work by the system to transport reactants and the product of the electrochemical reaction between the fuel channel and the reaction sites within the anode. Therefore, both anode and cathode concentrations do not contribute to the heat generated as shown in Figure-4. In Figure-4, the heat generated from the electrochemical reaction contributes the most heat generated as compared to the heat generated due to voltage losses (except concentration losses) during operation of the cell. Nevertheless, no significant difference in terms of the heat generated from the electrochemical reaction is found as the total amount of mole of supplied hydrogen within all fuel mixtures is the same. On the other side, it is found that the cell with a low hydrogen molar fraction generates more heat from voltage losses (except concentration loss). Among the waste heat that is generated due to voltage losses, ohmic loss contributes the most heat.

The high heat generated within a cell with an adiabatic thermal boundary generally leads to high average cell temperature as shown in Figure-3. High average cell temperature for the cell with a low hydrogen molar fraction within the supplied fuel mixture as discussed previous is found to contradict its low performance as shown in Figure-2. High temperature leads to low activation and ohmic losses as discussed by Yahya *et al.* [1] and Tan *et al* [6]. Nonetheless, such an advantage is overridden by the high anode concentration loss as shown in Figure-3. Figure-6 shows the distribution of pressure within the fuel channel at the fuel utilization of 75%. It is found that the strategy to maintain the same amount of mole for the supplied hydrogen within the fuel mixture leads to high total pressure at the inlet of the fuel channel. A high mass flow rate of the fuel mixture for the low molar fraction of hydrogen requires high flow energy that is reflected in high supplied pressure as shown in Figure-6(a). The partial pressure of gas species i p_i is related to its molar fraction x_i and total pressure P under the relationship of $p_i = x_i P$. As a result of the low molar fraction of hydrogen within the fuel mixture, it leads to the low partial pressure of hydrogen for the low molar fraction of the hydrogen fuel mixture in Figure-6(b). Such low partial pressure of hydrogen within the fuel channel leads to a high concentration loss in the anode and suppresses the positive effect of high average cell temperature within the cell.

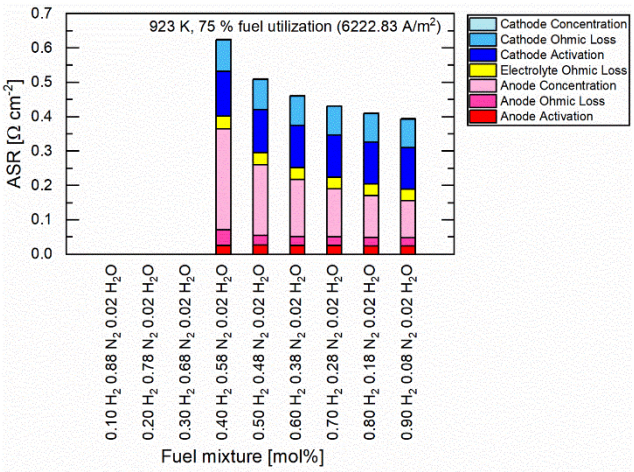

Figure-3. ASR analysis on the fuel mixture at 75 % fuel utilization.

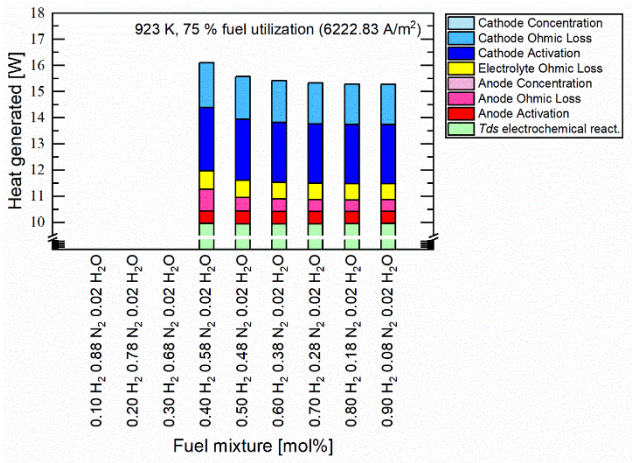

Figure-4. The heat generated at 75 % fuel utilization.

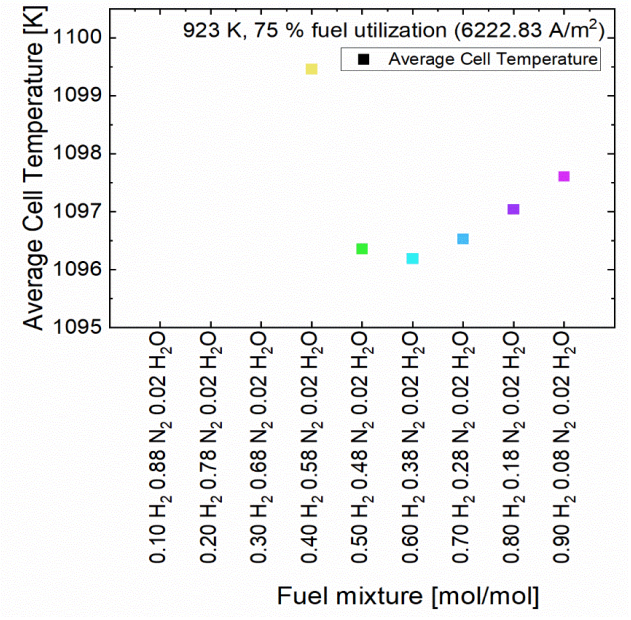

Figure-5. Average cell temperature at 75 % fuel utilization.

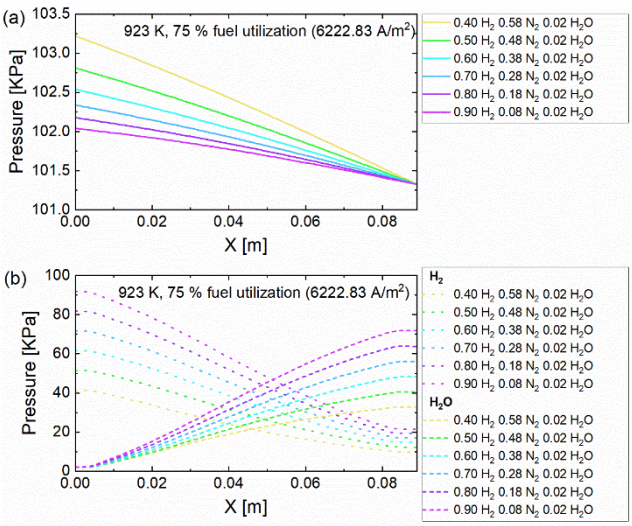

Figure-6. Pressure distribution in fuel channel at 75 % fuel utilization. (a) Total pressure, (b) Partial pressure of hydrogen and steam.

4. CONCLUSIONS

A quasi-3D SOFC model with real microstructure information is used to analyse the hydrogen-nitrogen-steam ternary fuel that is supplied to an SOFC under a fixed amount of hydrogen. The fuel mixture with a rich H_2 ratio (0.90 H_2: 0.08 N_2: 0.02 H_2O) shows an excellent performance among all fuel mixtures as the cell has the lowest total ASR value. Low heat generated from a low ASR SOFC unsuccessfully suppresses the cell performance as the high concentration of hydrogen within the supplied fuel greatly reduces the anode concentration over potential. Although this concentration over potential does not contribute towards the heat generated within a cell.

Credit authorship contribution statement

W. C. Tan: Conceptualization, Methodology, Validation, Formal analysis, Investigation, Writing - original draft, Writing - review & editing, Visualization. E. A. Lim: Software, Formal analysis, Investigation, Writing - review & editing. E. Meng Cheng: Formal analysis, Writing - original draft, Visualization. W. H. Tan: Investigation, Writing - review & editing. H. A. Rahman: Writing - review & editing, Proofreading.

REFERENCES

[1] A. Yahya, D. Ferrero, H. Dhahri, P. Leone, K. Slimi, M. Santarelli. 2018. Electrochemical performance of solid oxide fuel cell: Experimental study and calibrated model, Energy. 142, 932-943. https://doi.org/10.1016/J.ENERGY.2017.10.088.

[2] Y. Wu, H. Liu, Y. Wang, L. An, X. Xu. 2022. Spatially resolved electrochemical performance and temperature distribution of a segmented solid oxide fuel cell under various hydrogen dilution ratios and electrical loadings, J. Power Sources. 536, 231477. https://doi.org/10.1016/J.JPOWSOUR.2022.231477.

[3] Y. Komatsu, G. Brus, S. Kimijima, J.S. Szmyd. 2012. Experimental study on the 300W class planar type solid oxide fuel cell stack: Investigation for appropriate fuel provision control and the transient capability of the cell performance, J. Phys. Conf. Ser. 395, 012162. https://doi.org/10.1088/1742-6596/395/1/012162.

[4] G. Brus, K. Miyawaki, H. Iwai, M. Saito, H. Yoshida. 2014. Tortuosity in a Porous Anode Electrode of Solid Oxide Fuel Cells Estimated From Saturation Currents and a Mass Transport Model in Comparison With a Real Micro-Structure. 265, 1-14.

[5] H. Iwai, Y. Yamamoto, M. Saito, H. Yoshida. 2011. Numerical simulation of intermediate-temperature direct-internal-reforming planar solid oxide fuel cell, Energy. 36, 2225-2234. https://doi.org/10.1016/j.energy.2010.03.058.

[6] W. C. Tan, H. Iwai, M. Kishimoto, G. Brus, J.S. Szmyd, H. Yoshida. 2018. Numerical analysis on effect of aspect ratio of planar solid oxide fuel cell fueled with decomposed ammonia, J. Power Sources. 384C, 367-378.

[7] W. C. Tan, H. Iwai, M. Kishimoto, H. Yoshida. 2018. Quasi-three-dimensional numerical simulation of a solid oxide fuel cell short stack: Effects of flow configurations including air-flow alternation, J. Power

Sources. 400, 135-146. https://doi.org/10.1016/j.jpowsour.2018.08.002.

[8] W. C. Tan, E. A. Lim, E. M. Cheng, W. H. Tan. 2022. Numerical Analysis of the Effect of Pore Size Toward the Performance of Solid Oxide Fuel Cell BT - Proceedings of the 11th International Conference on Robotics, Vision, Signal Processing and Power Applications, in: N.M. Mahyuddin, N.R. Mat Noor, H.A. Mat Sakim (Eds.), Springer Singapore, Singapore. pp. 150-155.

[9] R. Jackson. 1977. Transport in porous catalysts, Elsevier Scientific Pub. Co., https://books.google.nl/books?id=bUNRAAAAMAAJ.

[10] E. N. Fuller, P. D. Schettler, J. C. Giddings. 1966. New method for prediction of binary gas-phase diffusion coefficients, Ind. Eng. Chem. 58, 18-27. https://doi.org/10.1021/ie50677a007.